Synergistic effect of essential oil distillates on the corrosion protection of GX4CrNiMo16-5-1 stainless in acid-chloride electrolyte

To cite this article: R T Loto 2022 *IOP Conf. Ser.: Mater. Sci. Eng.* **1222** 012005

Synergistic effect of essential oil distillates on the corrosion protection of GX4CrNiMo16-5-1 stainless in acid-chloride electrolyte

R T Loto[1]

Department of Mechanical Engineering, Covenant University, Ogun state, Nigeria

Email: tolulope.loto@covenantuniversity.edu.ng

Abstract. The inhibition capability of admixed rosemary oil with cinnamon cassia oil (RC), and grapefruit oil with lemongrass oil (GL) on GX4CrNiMo16-5-1 martensitic stainless steel (GX4ST) corrosion was studied in 6 M H_2SO_4/3.5% NaCl electrolyte by potentiodynamic polarization and optical microscopy characterization. Results show both admixed distillates performed effectively on GX4ST. The corrosion rate of GX4ST without the distillates at 2.82 mm/y significantly decreased to average value of 0.04 mm/y and 0.05 mm/y analogous to average inhibition efficiency of 98.64% and 98.23% for RC and GL compound. The oil distillates exhibit consistent anodic corrosion inhibition behavior at all concentrations studied. Corrosion thermodynamic calculations showed the distillates chemisorbed on the martensitic steel with Gibbs free energy values greater than -46.01 $Kjmol^{-1}$ with respect to Langmuir isotherm equation which indicates negligible of lateral interaction effect among inhibitor molecules and surface coverage protection mechanism. Optical image representations of GX4ST after corrosion without the distillates showed severe surface degradation of general and localized corrosion. This contrast the images of the inhibited steel surface which were closely similar to the steel image before corrosion.

1. Introduction

The consequences of corrosion of metallic alloys is enormous [1]. The most widely used metallic alloys are ferrous based especially stainless steels. Significant number of manufactured products consists of stainless steel. Stainless steels are recyclable, exhibits excellent mechanical properties, interfacial equilibrium, and thermal deformation resistance [2-4]. The steels are extensively utilized for structural application in nuclear, chemical processing, desalination, fertilizer production and petrochemical industries by reason of their extraordinary resilience against corrosion compared to carbon steels [5, 6]. The resilience of stainless steels against corrosion is due to the evolution of an insulating and inert oxide film on the steel. The oxide results from the presence of alloying elements within the steel metallurgical structure especially Cr and Ni which chemically combines with dissolved O_2 to passivate the steel surface. Electrochemical reaction of stainless steels with anions such as SO_4^{2-}, Cl^-, $S_2O_3^{2-}$, NO^-_3 etc. reacts with the outer electrons on the steel's exterior destabilizing the protective film especial at regions with flaws and discontinuities. Circumstances resulting in the disintegration of the protective oxide on stainless steels are prevalent in astringent industrial conditions couples with extreme temperature and high velocity fluid movement. Sequel to the collapse of passive films localized corrosion degradation majorly responsible for failure of stainless steels initiates and progresses [7, 8]. Pitting corrosion occurs

due to the evolution and increase in microscopic holes on stainless steel exterior which is significantly destructive to the operational lifespan of the steel in service especially in aqueous environments [9, 10]. The existence of SO_4^{2-} and Cl^- anions in aqueous environments causes instability of the protective oxide on steels leading to selective deterioration i.e. pitting corrosion [11]. The electrochemical performance of stainless steels analogous to the evolution, resilience and disintegration of their passive film is fundamental to the comprehension of the pitting corrosion resilience of these alloys. Mitigation against pitting corrosion is affiliated with cost consequences due to repair of metallic structures and components, and sustainability of their lifespan and reliability. Pitting corrosion is acute, insidious and undetectable which increases the difficulty to predict and design against [12]. Research on pitting corrosion evolution and progression on stainless steels have provided insight to the present understanding of its phenomena and have contributed to appropriate material selection for industrial application [13-18]. Yi et al [19] evaluated the pitting resistance of type 316 steel in specific chloride solutions and established that the critical pitting potential of the steel substantially depends on induced electrochemical factors. Hodge and Wilde [20] ascertained that Ni-Cr alloys (10% Cr content) exhibited passivation coupled with adequate resilience against pitting in sulphate-chloride solution. Piron et al [21] also ascertained correlating behavior between Ni 200 and Inconel 600 steel in sulphate solution. Friend [22] studied the disintegration of the insulating film on alloy 22 at critical chloride concentration. Investigation on metastable and stable pit propagation coupled with the influence of electrochemical factors have seen considerable progress with several mechanisms proposed to explain collapse of the passive film [23-27]. The resilience of these alloys against the damaging effect anionic species largely depends on the attributes and composition of their insulating film, repassivation tendency, metastable pitting behaviour and resilience to pitting corrosion. The ability of the protective oxide on stainless steels to with stand collapse and/or repassivate after breakdown in aqueous corrosive environments strongly influences the resilience of the steels to pitting corrosion. This can be significantly improved upon through the utilization of chemical fluids identified as corrosion inhibitors. Corrosion inhibitors substantially decrease the corrosion rate of metallic alloys in corrosive fluids [28, 29]. Inhibitors exhibit definite reaction behaviour analogous to specific alloys, industrial condition, concentration range etc. which influences their effectiveness. Traditional corrosion inhibitors (e.g. chromates, nitrates, nitrites, arsenic, phosphates etc.) are toxic [30-32]. Compounds of organic origin are proven alternatives but expensive and slightly toxic [33-39]. The relevance of sustainable, safe and cost-effective compounds cannot be overemphasized. Plants distillates have shown in previous research to be promising [40-42]. However, their inhibition performance against localized corrosion reaction phenomena needs to be ascertained. This manuscript focusses on the effect of plant distillates on the pitting corrosion evaluation and inhibition of GX4CrNiMo16-5-1 martensitic stainless steel.

2 Experimental methods

GX4CrNiMo16-5-1 martensitic stainless-steel plate (GX4ST) was acquired from Vienna University of Technology, Austria with average nominal (wt.%) content laid out in Table 1. The steel plate was cut to 12 test pieces with average dimension of 1 cm^3. They were subsequently smoothened with emery papers with 120, 240, 320, 600, 800, 1200 and 2500 grit before being washed with deionized H_2O and acetone. Grapefruit and lemon oil distillates were combined in ratio 1:1 and concocted in cubic concentrates of 1%, 2%, 3%, 4% and 5% in 200ml of 6M H_2SO_4/3.5% NaCl electrolyte while rosemary and cinnamon cassia were combined in ratio 1:1 and similarly prepared.

Table 1. Nominal (wt. %) content of GX4ST

Element	C	Si	Mn	P	S	Cr	Mo	Ni	Ti	N	Cu	V	Fe
Content	0.06	0.8	1	0.04	0	17	1.5	6	0	0	0.3	0.1	73.21

Potentiodynamic polarization investigations were executed with a triple electrode cable design inside a beaker filled with 200 mL of the electrolyte and joined to Digi-Ivy 2311 potentiostatic device. GX4ST

electrodes encased in solidified resin with visible surface area of 1 cm^2. Polarization plots were observed at sweep rate of 0.0015V/s from set potential of −0.5V and +1.5V. Pt wire was engaged as the counter electrode and Ag/AgCl as the standard electrode. Corrosion current density, J_c (A/cm^2) and corrosion potential, E_c (V) data were gotten from Tafel estimation approach. The corrosion rate C_R, (mm/y) and the inhibition efficiency, η (%) were computed from the numerical formula;

$$C_R = \frac{0.00327 \times J_c \times E_q}{D} \quad (1)$$

D represents density (g/cm^3) E_q represents equivalent of GX4ST. 0.00327 represents corrosion rate constant for computations in mm/y. Optical microscopy analysis was done with Omax trinocular metallurgical microscope for morphological analysis of the steel surface.

3 Results and discussion

3.1 Potentiodynamic polarization studies

Potentiodynamic polarization plots of GX4ST corrosion in 6M H_2SO_4/3.5% NaCl solution at 1-5% RC and GL concentration are laid out in Fig. 1(a) and (b). Table 2 exhibits the polarization data obtained. The corrosion rate of GX4ST at 0% RC and GL concentration (2.82 mm/y relating to corrosion current density of 2.62 x 10^{-4}A/cm^2) significantly differs from the values obtained at 1-5% concentration of the inhibitors preceding from oxidation of the steel surface by SO_4^{2-} and Cl^- anions. The anions are responsible for the release of Fe^{2+} ions into the acid-chloride electrolyte coupled with Cr depletion on the steel's protective film. Consequentially, the chemical fusion of H_2 atoms leads to evolution of H_2 gas and O_2 reduction reactions which are also responsible for selective degradation of the steel. Observation of GX4ST polarization plots at 0% inhibitor concentration in Fig. 1(a) and (b) shows the anodic-cathodic polarization slopes are substantially greater than the slopes at other inhibitor concentration due to action redox reaction mechanism during potential scanning. At 1% RC concentration in Fig. 1(a), significant decrease in the anodic-cathodic plot configuration are visible due to interference and suppression of the redox reaction mechanism. This observation coincides with corrosion rate of 0.03 mm/y and corrosion current density of 3.04 x 10^{-6} A/cm^2. RC concentration had negligible effect on its inhibition performance with inhibition efficiency result remaining generally similar. This proves the inhibition performance of RC is concentration dependent. This claim is proven from the similarities in configuration of the anodic polarization plots at 1-5% RC concentration and the cathodic plots at 2-5% RC concentration. It signifies the inhibition performance of RC is under activation control due to stability of the inhibition action and behaviour of RC analogous to concentration. Corrosion rate of GX4ST varies between 0.03 mm/y and 0.04 mm/y while the inhibition efficiency varies between 98.84% and 98.53%. The corrosion potential of the polarization plots at specific RC concentration tends to electropositive values due to dominant anodic inhibition behaviour. However, the optimal difference between the corrosion potential of GX4ST polarization plot at 0% RC and specific RC concentration is 103 mV signifying RC exhibits anodic inhibition behaviour. This shows that protection of the steel by protonated RC molecules occurred through adsorption. This is further confirmed from the pseudo passivation behaviour of the anodic polarization plots.

The performance of GL inhibitor is generally similar to RC with respect to corrosion rate and inhibition efficiency values, which varied between values of 0.06 mm/y – 0.04 mm/y and 97.94% - 98.71%. However, variation of the anodic-cathodic plots with respect to GL concentration shows GL inhibition behaviour steers significantly away from activation control mechanism. The slopes of the plot configuration show the mechanism of GL inhibition is significantly influenced by the redox reactions taking place on the steel surface. The deviation in corrosion potential to electropositive values shows GL inhibits GX4ST surface through surface coverage with optimal difference in corrosion potential between GL inhibited steel and the steel at 0% GL concentration is 90 mV which shows GL is also an anodic type inhibitor. Comparing the performance of the inhibitor compounds it's clearly visible that the performance of the inhibitors is generally similar and highly effective.

Table 2. Potentiodynamic polarization output of GX4ST corrosion in 6 M H_2SO_4/3.5% NaCl solution at 1-5% RC and GL concentration

RC Inhibitor									
Sample	**RC Conc. (%)**	**LCS C_R (mm/y)**	**RC ξ_F (%)**	**C_I (A)**	**C_J (A/cm^2)**	**C_P (V)**	**R_p (Ω)**	**B_c (V/dec)**	**B_a (V/dec)**
A	0	2.82	0	2.96E-04	2.62E-04	-0.364	86.73	-9.115	12.490
B	0.5	0.03	98.84	3.44E-06	3.04E-06	-0.261	7479.00	-8.635	13.370
C	1	0.04	98.53	4.36E-06	3.86E-06	-0.328	5894.00	-7.056	9.081
D	1.5	0.03	98.91	3.23E-06	2.86E-06	-0.310	7961.00	-5.662	9.139
E	2	0.04	98.41	4.71E-06	4.17E-06	-0.285	5450.70	-7.698	13.167
F	2.5	0.04	98.53	4.37E-06	3.86E-06	-0.285	5886.00	-7.149	11.300
GL Inhibitor									
Sample	**RCC Conc. (%)**	**LCS C_R (mm/y)**	**RCC ξ_F (%)**	**C_I (A)**	**C_J (A/cm^2)**	**C_P (V)**	**R_p (Ω)**	**B_c (V/dec)**	**B_a (V/dec)**
A	0	2.82	0	2.96E-04	2.62E-04	-0.364	86.73	-9.115	12.490
B	0.5	0.06	97.94	5.74E-06	5.08E-06	-0.274	4477.00	-10.660	28.710
C	1	0.05	98.06	5.42E-06	4.79E-06	-0.282	4815.00	-11.550	14.290
D	1.5	0.06	97.99	5.63E-06	4.98E-06	-0.324	5387.80	-9.321	12.600
E	2	0.04	98.43	4.38E-06	3.88E-06	-0.342	6078.00	-10.290	14.000
F	2.5	0.04	98.71	3.59E-06	3.18E-06	-0.274	7158.00	-9.496	25.270

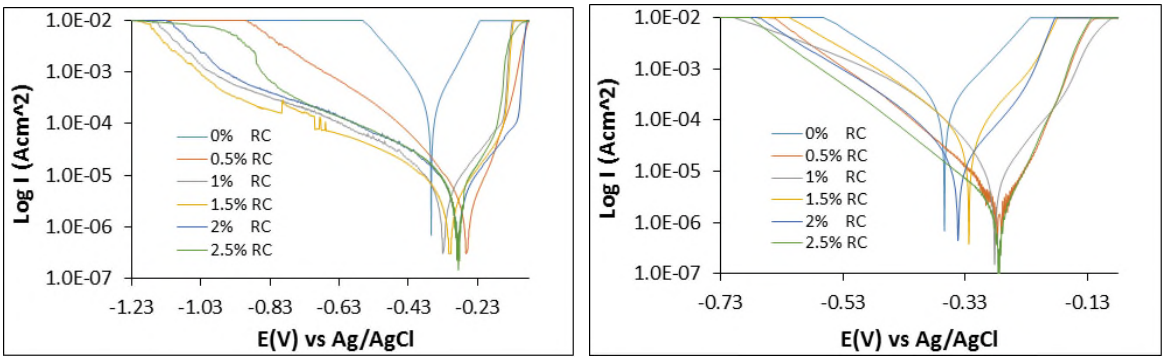

(a) (b)

Figure. 1 Potentiodynamic polarization plots of GX4ST corrosion in 6 M H2SO4/3.5% NaCl solution at 1-5% (a) RC concentration and (b) GL concentration

3.2 Corrosion thermodynamic studies

Adsorption isotherms provide insight into the mechanism of inhibitor-metal interaction leading to stifling of the redox reactions identified with corrosion. Inhibitor protection of metallic alloys occurs through electrostatic attraction between protonated inhibitor molecules in the electrolyte solution and valence electrons on the ionized steel surface. Strong electrostatic attraction culminates in effective corrosion inhibition. However, this assertion is subject to the ionic behaviour of corrosive species as most organic corrosion inhibitors depends on preadsorption of the corrosive species onto the steel before electrostatic attraction of the inhibitor onto the steel surface. Secondly, the organo-metallic complexation is also an important factor i.e. covalent bonding between the RC/GL molecules and the ionized steel surface stifles the corrosion reaction mechanisms. This reaction mechanism is termed chemisorption. In cases where the bonding is weak, it falls under Van der Waals interaction termed physisorption [43]. Data obtained from potentiodynamic polarization was evaluated with conventional adsorption isotherms. Only Langmuir isotherm models prove to be most applicable with interaction coefficients greater than 0.9 for RC and GL inhibitors. The interaction coefficient values are laid out in Table 3 below;

Table 3. Analogy of interaction coefficient values for Langmuir isotherm in 6 M H_2SO_4/3.5% NaCl for RC and GL inhibitor

Adsorption Isotherm	RC Inhibitor	GL Inhibitor
Langmuir	1	0.9999

The Langmuir isotherm plots obtained from the fluid electrolyte in the presence of the inhibitors are presented in Figs. 2(a) and (b). Langmuir isotherm indicates that adsorption of inhibitor molecules occurs at the same definite reaction sites in the absence lateral interaction among inhibitor molecules with respect to mono layer adsorption according to the equation below;

$$\theta = \left[\frac{K_{\text{ads}}C_{\text{Inh}}}{1+K_{\text{ads}}C_{\text{Inh}}}\right] \quad (2)$$

K_{ads} represents equilibrium constant of adsorption and C_{Inh} represents molar concentration of inhibitor compound [44].

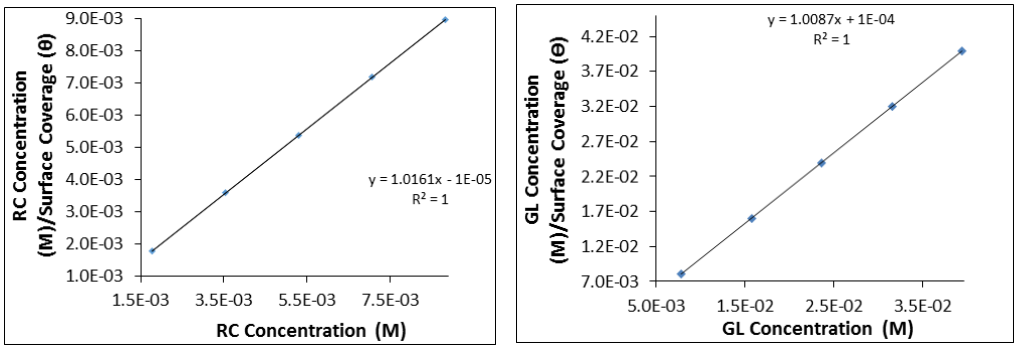

(a) (b)

Figure. 2 Langmuir adsorption isotherm plots from 6 M H_2SO_4/3.5% NaCl solution in the presence of (a) RC inhibitor and (b) GL inhibitor

Data output of Gibbs free energy (ΔG) calculated from equation 5 are displayed in Table 4. The data indicates the nature, potency and stability of adsorption mechanism of RC and GL inhibitor on GX4ST in the acid-chloride solution. The equilibrium constant of adsorption (K_{ads}) was computed from Langmuir isotherm equation.

$$\Delta G_{\text{ads}} = -2.303RT \log [55.5K_{\text{ads}}] \quad (3)$$

55.5 indicate molar concentration of H_2O in the acid solution, *R* indicates universal gas constant and *T* indicates absolute temperature. The ΔG data from the acid solutions in the presence of RC and GL inhibitors shows the inhibitor interaction mechanism occur through chemisorption adsorption [45]. The ΔG values associated with RC inhibition action are slightly higher than the corresponding values for GL inhibitor which signifying higher adsorption strength. The general slight decrease in value in the presence of both inhibitors results from lateral repulsion effect between protonated inhibitor molecules which in effect is negligible.

Table 4. Data output for Gibbs free energy (ΔG) and equilibrium constant of adsorption (K_{ads}) for RC and GL adsorption on GX4ST in 6 M H_2SO_4/3.5% NaCl

			RC Inhibitor			GL Inhibitor		
GX4ST Samples	**Inhibitor Conc. (%)**	**Inhibitor Conc. (M)**	**Surface Coverage (θ)**	**Equilibrium Constant of adsorption (K)**	**Gibbs Free Energy, ΔG (Kjmol^{-1})**	**Surface Coverage (θ)**	**Equilibrium Constant of adsorption (K)**	**Gibbs Free Energy, ΔG (Kjmol^{-1})**
A	0	0	0	0	0	0	0	0
B	0.5	1.77E-03	0.988	48278217.5	-53.79	0.971	4291032.0	-47.80
C	1	3.53E-03	0.985	18967843.5	-51.48	0.990	6149334.6	-48.69
D	1.5	5.30E-03	0.989	17147218.5	-51.23	0.988	3468913.5	-47.27
E	2	7.07E-03	0.984	8770399.9	-49.57	0.989	2770338.8	-46.71
F	2.5	8.84E-03	0.985	7576552.8	-49.21	0.988	2087012.9	-46.01

3.3 Optical image analysis

Optical images of GX4ST prior to and after corrosion assessment are exhibited from Fig. 3(a) to 5(b). Fig. 3(a) presents the image after metallographic preparation prior to corrosion test. Fig. 3(b) shows the morphology of GX4ST after corrosion in 6M H_2SO_4/3.5% NaCl. Extensive surface degradation is clearly visible due to oxidation of the steel exterior by the corrosive action of SO_4^{2-} and Cl^- anions. Corrosion pits are also visible due to localized electrochemical deterioration at definite areas on the steel where the passive protective film weakened. Fig. 4(a) to 5(b) exhibits the morphology of GX4ST after corrosion in the presence of 1% and 5% RC and GL concentrations respectively. The morphologies show effective inhibitor protection as they contrast the degraded morphology in Fig. 3(b). The corrosive anions where hindered from diffusing unto and reacting with the steel surface. However, miniature surface degradation and corrosion pits are still partially visible due to preadsorbed corrosive anions which aided the electrostatic attraction of the protonated inhibitor molecules. However, the surface morphology of the inhibited steels is well protected and assents with the results from potentiodynamic polarization.

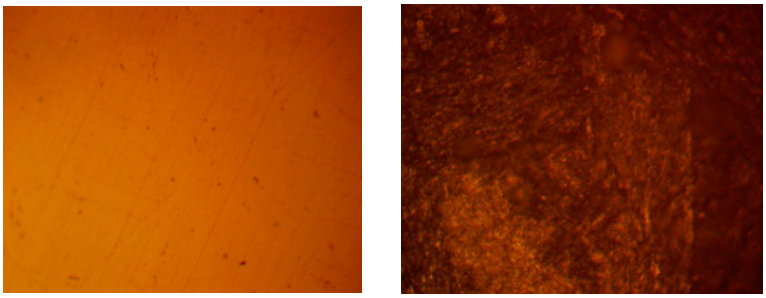

(a) (b)

Figure. 3 Optical images of GX4ST (a) prior to corrosion analysis and (b) after corrosion from 6 M H_2SO_4/3.5% NaCl solution

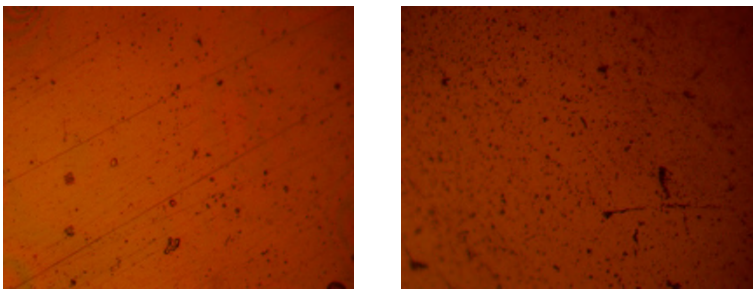

(a) (b)

Figure. 4 Optical images of GX4ST after corrosion from 6 M H_2SO_4/3.5% NaCl solution at (a) 1% RC concentration and (b) 1% GL concentration

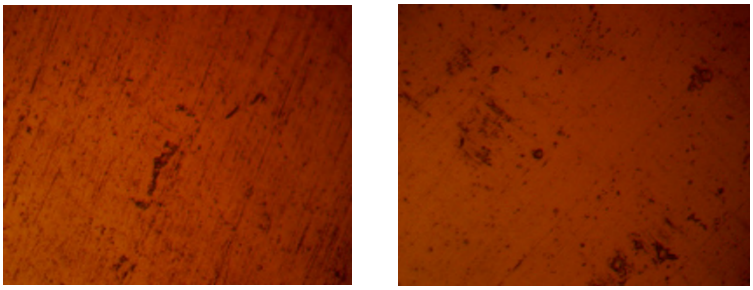

(a) (b)

Figure. 5 Optical images of GX4ST after corrosion from 6 M H_2SO_4/3.5% NaCl solution at (a) 6% RC concentration and (b) 6% GL concentration

4. Conclusion

Admixture of rosemary oil with cinnamon cassia oil, and grapefruit oil with lemongrass oil effectively inhibited the corrosion of GX4CrNiMo16-5-1 martensitic stainless steel in chloride-sulphate solution. Both admixed oil distillates performed adequately at specific concentrations with inhibition efficiency values generally signifying stability of the inhibitive electrochemical behavior of the oil distillates in the electrolyte. The admixed oil distillates exhibited anodic type inhibition effect resulting in surface coverage over the entire steel. The oil distillates adsorbed onto the steel by chemisorption reaction process through covalent bonding and strong electrostatic attraction. Optical images of the inhibited steel significantly differ from the non-inhibited and corroded steel due to absence of protonated oil distillates to counterbalance the combined destructive effect of chlorides and sulphates in the electrolyte.

Acknowledgement

The author recognizes the support of Covenant University Ota, Ogun State, Nigeria for this research.

References

[1] Palaniswamy BRN, Rengaswamy NS and Jayachandran M (2005) A review of differing approaches used to estimate the cost of corrosion (and their relevance in the development of modern corrosion prevention and control strategies) *Anti Corros. Method M* **52(1)** 29-41.
[2] Reuter MA, Heiskanen K, Boin U, Van Schaik A, Verhoef E, Yang Y and Georgalli G (2005) The metrics of material and metal ecology, Harmonizing the resource, technology and environmental cycles, Elsevier Science Vol. 16.
[3] Christopher R (2011) Sustainability and value of steel recycling in Uganda *J. Civ. Eng. Constr. Technol.* **2(10)** (2011).
[4] Tan Q and Li J (2015) Recycling metals from wastes: A novel application of mechanochemistry *Environ. Sci. Technol.* **49(10)** 5849–5861.
[5] Caron P and Khan T (1999) Evolution of Ni-Base Superalloys for single crystal gas turbine blade applications *Aerosp. Sci. Technol*. **3** 513-523.
[6] Hashizume R, Yoshinari A, Kiyono T, Murata Y and Morinaga M (2007) Development of Ni-based single crystal superalloys for power generation gas turbines *Energ. Mater. Mater. Sci. Eng. Energ. Syst.* **2(1)** 5-12.
[7] McCafferty E (2003) Sequence of steps in the pitting of aluminum by chloride ions *Corros. Sci.* **45** 1421-1438.
[8] Abdel Rehim SS, Hassan HH and Amin MA (2004) Chronoamperometric studies of pitting corrosion of Al and (Al–Si) alloys by halide ions in neutral sulphate solutions *Corros. Sci*. **46** 1921-1938.
[9] Loto RT and Loto CA (2017) Corrosion behaviour of S43035 ferritic stainless steel in hot sulphate/chloride solution *J. Mater. Sci. Technol*. doi.org/10.1016/j.jmrt.2017.07.004.
[10] Li S, Xu Y, Li H and Guan X (2014) Uniform and pitting corrosion modeling for high-strength bridge wires *J. Bridge Eng.* **19(7)**. doi.org/10.1061/(ASCE)BE.1943-5592.0000598
[11] Nieuwoudt MK, Comins JD and Cukrowski I (2012) Analysis of the composition of the passive film on iron under pitting conditions in 0.05 M NaOH/NaCl using Raman microscopy in situ with anodic polarisation and MCR-ALS *J. Raman Spectrosc.* **43(7)** (2012), p. 928-938. doi.org/10.1002/jrs.3109.
[12] Guo P, La Plante EC, Wang B, Chen X, Balonis M, Bauchy M and G. Sant G (2018) Direct observation of pitting corrosion evolutions on carbon steel surfaces at the nano-to-micro- scales *Sci. Rep.* 8(7990). doi.org/10.1038/s41598-018-26340-5
[13] Loto RT and Loto CA (2017) Potentiodynamic polarization behavior and pitting corrosion analysis of 2101 duplex and 301 austenitic stainless steel in sulfuric acid concentrations *J. Fail. Anal. Prev*. **17(4)** 672–679.
[14] Loto RT and Loto CA (2015) Pitting corrosion inhibition of type 304 austenitic stainless steel by 2 amino 5 ethyl 1,3,4 thiadiazole in dilute sulphuric acid Prot Met Phys Chem+ 51(4) (2015), p. 693–700.
[15] Loto RT (2013) Pitting corrosion evaluation of austenitic stainless steel type 304 in acid chloride media *J. Mats. & Environ. Sci*. **4(4)** 448-459.
[16] Tian W, Du N, Li S, Chen S and Wu Q (2013) Metastable pitting corrosion of 304 stainless steel in 3.5% NaCl solution *Corros. Sci*. **85** 372-379.
[17] Yi Y, Cho P, Al Zaabi A, Addad Y and Jang C (2013) Potentiodynamic polarization behaviour of AISI type 316 stainless steel in NaCl solution *Corros. Sci*. **74** 92–97.
[18] Hodge FG and Wilde BE (1970) Effect of chloride ion on the anodic dissolution kinetics of chromium–nickel binary alloys in dilute sulfuric acid *NACE Corrosion* **26(6)** 246-250.
[19] Piron DL, Koutsoukos EP and Nobe K (1969) Corrosion behavior of nickel and inconel in acidic chloride solutions *NACE Corrosion* **25(4)** 151-156.
[20] Friend WZ (1980) Nickel-Chromium-Molybdenum Alloys, Wiley-Interscience, New York.

[21] Pahlavan S, Moazen S, Taji I, Saffar K, Hamrah M, Moayed MH, Mollazadeh S and Beidokhti S (2016) Pitting corrosion of martensitic stainless steel in halide bearing solutions *Corros. Sci*. **112** 233–240.
[22] Lu K and Lu J (2004) Nanostructured surface layer on metallic materials induced by surface mechanical attrition treatment *Mater. Sci. Eng. A*. **375-377** 38-45.
[23] Pistorius PC and Burstein GT (1992) Metastable Pitting Corrosion of Stainless Steel and the Transition to Stability *Philos. Trans.: Phys. Sci. Eng*. **341** 531–559.
[24] Pistorius PC and Burstein GT (1992) Growth of corrosion pits on stainless steel in chloride solution containing dilute sulphate *Corros. Sci*. **33** 1885–1897.
[25] Ernst P, Laycock NJ, Moayed MH, Newman RC (1997) The mechanism of lacy cover formation in pitting *Corros. Sci*. **39** 1133–1136.
[26] Laycock NJ and Newman RC (1998) Temperature dependence of pitting potentials for austenitic stainless steels above their critical pitting temperature *Corros. Sci.* **40** 887–902.
[27] Soltis J (2015) Passivity breakdown, pit initiation and propagation of pits in metallic materials – Review *Corros. Sci*. **90** 5–22.
[28] Popov BN (2015) Chapter 14 - Corrosion Inhibitors, Corrosion Engineering Principles and Solved Problems, Elsevier Inc., Amsterdam, pp. 581-597. https://doi.org/10.1016/B978-0-444-62722-3.00014-8.
[29] Palanisamy G (2018) Corrosion Inhibitors, IntechOpen. http://doi.org/10.5772/intechopen.80542.
[30] Sastri VS (2014) Types of corrosion inhibitor for managing corrosion in underground pipelines, Underground Pipeline Corrosion, Elsevier Inc., Amsterdam, pp. 166-211. https://doi.org/10.1533/9780857099266.1.166.
[31] Chen Y and Yang W (2019) Formulation of Corrosion Inhibitors. http://doi.org/ 10.5772/intechopen.88533.
[32] Dariva CG and Galio AF (2013) Corrosion Inhibitors – Principles, Mechanisms and Applications, IntechOpen. http://doi.org/10.5772/57255.
[33] Ahmed SK, Ali WB and Khadom AA (2019) Synthesis and investigations of heterocyclic compounds as corrosion inhibitors for mild steel in hydrochloric acid *Int. J. Ind. Chem*. **10** 159–173.
[34] Singh A, Talha M, Xu X, Sun Z and Lin Y (2017) Heterocyclic corrosion inhibitors for J55 steel in a sweet corrosive medium *ACS Omega* **2(11)** 8177-8186.
[35] Singh A, Ansari KR, Quraishi MA, Kaya S and Banerjee P (2019) The effect of an N-heterocyclic compound on corrosion inhibition of J55 steel in sweet corrosive medium *New J. Chem*. **43** 6303-6313.
[36] Sundaram RG and Sundaravadivelu M (2016) Anticorrosion Activity of 8-Quinoline Sulphonyl Chloride on Mild Steel in 1 M HCl Solution *Journal of Metallurgy* 8095206. https://doi.org/10.1155/2016/8095206.
[37] Loto RT (2017) Study of the synergistic effect of 2-methoxy-4-formylphenol and sodium molybdenum oxide on the corrosion inhibition of 3CR12 ferritic steel in dilute sulphuric acid *Results in Phys*. **7** 769-776.
[38] Loto CA and Loto RT (2013) Effect of dextrin and thiourea additives on the zinc electroplated mild steel in acid chloride solution *Int. J. Elect. Sci.* **8(12)** 12434-12450.
[39] Loto RT and Loto CA (2012) Effect of P-phenylediamine on the corrosion of austenitic stainless steel type 304 in hydrochloric acid *Int. J. Elect. Sci*. **7(1)** 9423-9440.
[40] Loto RT, Leramo R and Oyebade B (2018) Synergistic combination effect of salvia officinalis and lavandula officinalis on the corrosion inhibition of low-carbon steel in the presence of SO_4^{2-} and Cl^- containing aqueous environment *J. Fail. Anal. Prev*. **18(6)** 1429-1438.
[41] Loto RT and Oghenerukewe E (2016) Inhibition studies of rosmarinus officinalis on the pitting corrosion resistance 439LL ferritic stainless steel in dilute sulphuric acid *Orient. J.Chem*. **32(5)** 2813-2832.

[42] Loto CA, Loto RT and Popoola API (2011) Effect of neem leaf (azadirachita indica) extract on the corrosion inhibition of mild steel in dilute acids *Int. J. Phy. Sci.* **6(9)** 2249-2257.
[43] Bockris JO and Swinkels DAJ (1964) Adsorption of n-decylamine on solid metal electrodes *J. of Elect. Soc*. **111(6)** 736.
[44] Vijayaraghavan K, Padmesh TVN, Palanivelu K and Velan M (2006) Biosorption of nickel (II) ions onto Sargassum wightii: Application of two-parameter and three parameter isotherm models *J. Hazard. Mater*. **B133** 304–308.
[45] Loto RT, Loto CA, Joseph O and Olanrewaju G (2016) Adsorption and corrosion inhibition properties of thiocarbanilide on the electrochemical behaviour of high carbon steel in dilute acid solutions *Results in Phys*. **6** 305-314. https://doi.org/10.1016/j.rinp.2016.05.013 (2016).